frontiers in Materials

ORIGINAL RESEARCH
published: 29 November 2018
doi: 10.3389/fmats.2018.00072

Superconducting $Ti_{15}Zr_{15}Nb_{35}Ta_{35}$ High-Entropy Alloy With Intermediate Electron-Phonon Coupling

Yuan Yuan[1], Yuan Wu[1], Huiqian Luo[2,3], Zhaosheng Wang[4], Xue Liang[5], Zhi Yang[1], Hui Wang[1], Xiongjun Liu[1] and Zhaoping Lu[1]**

[1] State Key Laboratory for Advanced Metals and Materials, University of Science and Technology Beijing, Beijing, China, [2] Beijing National Laboratory for Condensed Matter Physics, Institute of Physics, Chinese Academy of Sciences, Beijing, China, [3] Songshan Lake Materials Laboratory, Dongguan, China, [4] High Magnetic Field Laboratory, Chinese Academy of Sciences, Hefei, Anhui, China, [5] Laboratory for Microstructures, Institute of Materials, Shanghai University, Shanghai, China

The body-centered cubic (BCC) $Ti_{15}Zr_{15}Nb_{35}Ta_{35}$ high-entropy alloy showed superconducting behavior at around 8 K. The electronic specific heat coefficient γ and the lattice specific heat coefficient β were determined to be $\gamma = 9.3 \pm 0.1$ mJ/mol K^2 and $\beta = 0.28 \pm 0.01$ mJ/mol K^4, respectively. It was found that the electronic specific heat C_{es} does follow the exponential behavior of the Bardeen-Cooper-Schrieffer (BCS) theory. Nevertheless, the specific heat jump ($\Delta C/\gamma T_c$) at the superconducting transition temperature which was determined to be 1.71 deviates appreciably from that for a weak electron-phonon coupling BCS superconductor. Within the framework of the strong-coupled theory, our analysis suggests that the$Ti_{15}Zr_{15}Nb_{35}Ta_{35}$ HEA is an intermediate electron-phonon coupled BCS-type superconductor.

Keywords: high-entropy alloys, superconducting, BCS-type, specific heat jump, intermediate electron-phonon coupled

OPEN ACCESS

Edited by:
John L. Provis, University of Sheffield, United Kingdom

Reviewed by:
Jacqueline Krim, North Carolina State University, United States
Alexander Petrovic, Nanyang Technological University, Singapore

***Correspondence:**
Yuan Wu
wuyuan@ustb.edu.cn
Zhaoping Lu
luzp@ustb.edu.cn

Specialty section:
This article was submitted to Structural Materials, a section of the journal Frontiers in Materials

Received: *04 July 2018*
Accepted: *09 November 2018*
Published: *29 November 2018*

Citation:
Yuan Y, Wu Y, Luo H, Wang Z, Liang X, Yang Z, Wang H, Liu X and Lu Z (2018) Superconducting $Ti_{15}Zr_{15}Nb_{35}Ta_{35}$ High-Entropy Alloy With Intermediate Electron-Phonon Coupling. Front. Mater. 5:72. doi: 10.3389/fmats.2018.00072

INTRODUCTION

Within the past decade, high-entropy alloys (HEAs) have attracted extensive attention due to their unique compositions, interesting microstructures, and promising properties. Traditional alloys usually contain one element as the principle constituent with some other minor elements incorporated for property optimization (Lu et al., 2015). However, HEAs contain at least four principle elements in equal or near-equal atomic ratio (Li et al., 2017). It is interesting to note that, despite containing a large number of components, HEAs tend to form simple face-centered cubic (FCC), body-centered cubic (BCC), and hexagonal close-packed (HCP) structure instead of complex phases and intermetallic compounds (Urban and Feuerbacher, 2004; Conrad et al., 2009). Most current studies are focusing on the relationship between microstructure and mechanical properties (Yeh et al., 2004; Yeh, 2006; Zhou et al., 2007; Wen et al., 2009; Senkov et al., 2010, 2011; Chuang et al., 2011; Hsu et al., 2011), but limited work on the physical properties. Recently, it was revealed that the $Ta_{34}Nb_{33}Hf_8Zr_{14}Ti_{11}$ HEA became a superconductor at 7.3 K in a weak electron-phonon coupled matter (Koželj et al., 2014), which attracted tremendous interests. Recently, it was reported that $(TaNb)_{0.67}(HfZrTi)_{0.33}$ HEA even showed a robust superconducting (SC) behavior under extreme pressure up to 160 GPa, a pressure like that within the outer core of the earth (Guo et al., 2017). Note that Ti, Zr, Nb, and Ta are known to be SC elements under ambient pressure, and proper mixing of these elements is favorable for a formation of a single solid solution

phase (Todai et al., 2017). Therefore, careful studies on the SC behavior of the Ti-Zr-Nb-Ta HEA system is interesting, which may offer new clues for understanding SC mechanism of HEAs. Herein, we report synthesis and characterization of a novel four-component $Ti_{15}Zr_{15}Nb_{35}Ta_{35}$ HEA with a SC transition temperature T_c ($T_c \approx 8$ K). Our analysis indicates that the $Ti_{15}Zr_{15}Nb_{35}Ta_{35}$ HEA is an intermediate electron-phonon coupled superconductor, which naturally explains its higher T_c in comparison with $Ta_{34}Nb_{33}Hf_8Zr_{14}Ti_{11}$ HEA compound.

MATERIALS AND METHODS

99.9% pure Ti, Zr, Nb, and Ta were used as starting materials for the preparation of alloy ingots with a nominal composition of $Ti_{15}Zr_{15}Nb_{35}Ta_{35}$ (at. %). The materials were put in a water-cooled copper crucible in a vacuum arc furnace. Then the materials were melted by an argon arc plasma flame at half atmospheric pressure under argon atmosphere. A dc power source with about 100 A was adjusted for 10 s and then increased to 300–400 A for about 1 min. The arc-flame between the tungsten electrode and the surface of the molten sample was maintained at about 20 mm during the arc melting process. The ingots were re-melted at least six times to ensure chemical homogeneity and subsequently drop-cast into a copper mold with a dimension of $\Phi 10 \times 60$ mm. Phase constituents were characterized by X-ray diffraction (XRD) using Cu-Kα radiation. Specific heat, resistivity and magnetization measurements were carried out on a physical property measurement system (PPMS) from Quantum Design Company.

RESULTS AND DISCUSSION

X-ray diffraction pattern of the as-cast $Ti_{15}Zr_{15}Nb_{35}Ta_{35}$ sample is shown in **Figure 1** in which all diffraction peaks can be indexed to a BCC lattice, indicating formation of a single crystalline phase in the current alloy. The lattice constant of the current HEA using Vegard's rule of mixture(Vegard, 1921), $a_{mix} = \sum_i c_i a_i$, which is valid for completely random mixing of the elements, was calculated to be $a = 3.340$ Å. Here c_i is atomic fraction and a_i is lattice parameter of the element i (**Table 1**) (Koželj et al., 2014).The calculated value is in good agreement with experimental value (i.e., a=3.329 Å, suggesting that the constituent elements are likely randomly mixed in the current BCC lattice.

Temperature dependence of electrical resistivity $\rho\,(T)$ in zero field is shown in **Figure 2**, and the inset shows the variation of resistivity as a function of temperature under magnetic field $\rho\,(T)\,H$ up to 10 T field. The resistivity value is 25 ± 1 $\mu\Omega$ cm at room temperature, and decreases with temperature as expected for metallic behavior(Awana et al., 2010). At 8 K, the $Ti_{15}Zr_{15}Nb_{35}Ta_{35}$ sample exhibits SC behavior, as the resistivity gradually approaches zero. The$\rho\,(T)\,H$ measurements reveal that the SC transition temperature is shifted to lower temperatures as the applied magnetic field is increases. **Figure 3** shows $C\,(T)$ of the $Ti_{15}Zr_{15}Nb_{35}Ta_{35}$ HEA in the magnetic field of 0, 4, 8, and10 T. An anomaly at about 8 K associated with the SC transition is visible in the magnetic field of 0 and 4 T, but disappear in the magnetic field of 10 T. This observation is in good agreement with the results of electrical resistivity $\rho\,(T)$ (shown in **Figure 2**).

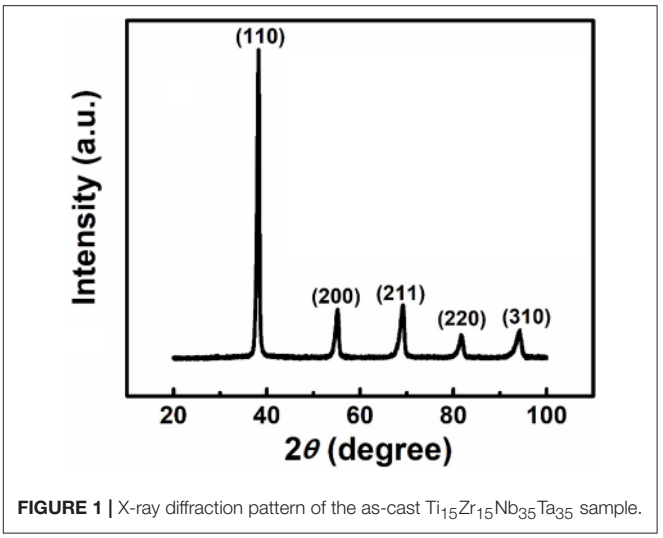

FIGURE 1 | X-ray diffraction pattern of the as-cast $Ti_{15}Zr_{15}Nb_{35}Ta_{35}$ sample.

TABLE 1 | Lattice constant a (Koželj et al., 2014), SC transition temperature T_C (Ashcroft and Mermin, 1976) and the specific heat coefficients γ (Tari, 2003) of pure constituent elements and the investigated $Ti_{15}Zr_{15}Nb_{35}Ta_{35}$ HEA.

	Ti	Zr	Nb	Ta	Theor.	Exp.
a(Å)	3.276	3.582	3.301	3.303	3.340	3.329
T_C(K)	0.40	0.61	9.25	4.47	4.95	8.00
γ(mJ/mol K^2)	3.36	2.77	7.80	5.87	5.70	9.30 ± 0.10

The theoretical values (HEA theor.) were calculated based on the "rule of mixtures."

Figure 4 shows temperature dependence of magnetic susceptibility $\chi\,(T)$ under zero-field-cooled (ZFC) and field-cooled (FC) conditions at 3 mT for the current $Ti_{15}Zr_{15}Nb_{35}Ta_{35}$ HEA. The susceptibility becomes negative (diamagnetic) below temperature 8.5 K, with a strong diamagnetic response due to the Meissner effect. Here, the measured χ_0 was corrected for demagnetization fields$\chi = \chi_0/(1 - D\chi_0)$, where χ is the susceptibility corrected for demagnetization, and D is the demagnetization factor. Exact value of D was obtainable only for ellipsoids. The ratio of length to diameter for our cylinder-like sample is about 0.6, then the average value of D for uniformly magnetized cylinders is 0.43 according to the results computed by Brown (1960) and Crabtree (1977). Thus, it can also be clearly observed that the value of magnetic susceptibility (χ) is about −1, corrected for the demagnetization factor. This observation indicates that the SC volume fraction is almost 100%. The left inset of **Figure 4** shows isothermal magnetization $M\,(H)$ curves at 3–10 K in the field range up to 80 kA/m. A linear response due to Meissner effect is observed with a slope nearly −1, which confirms the bulk superconductivity. Then the magnitude of M decreases with increasing H, which is typical in the vortex

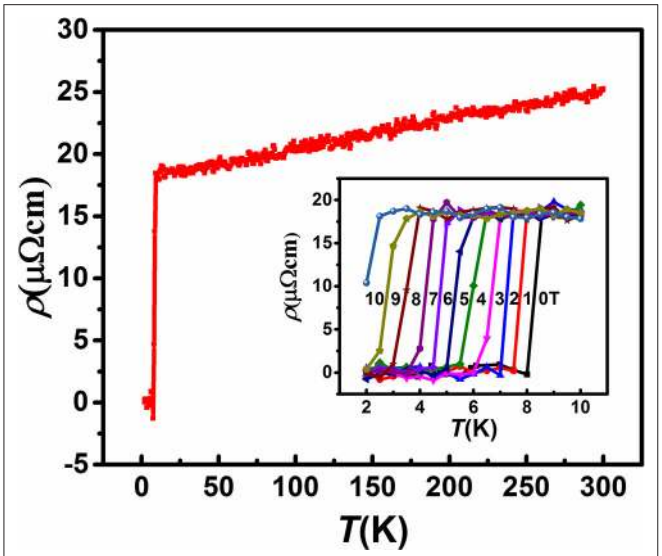

FIGURE 2 | Temperature dependence of electrical resistivity $\rho\,(T)$ in zero field of the $Ti_{15}Zr_{15}Nb_{35}Ta_{35}$ HEA. The inset shows the variation of resistivity as a function of temperature under magnetic field $\rho\,(T)\,H$ up to10 T field.

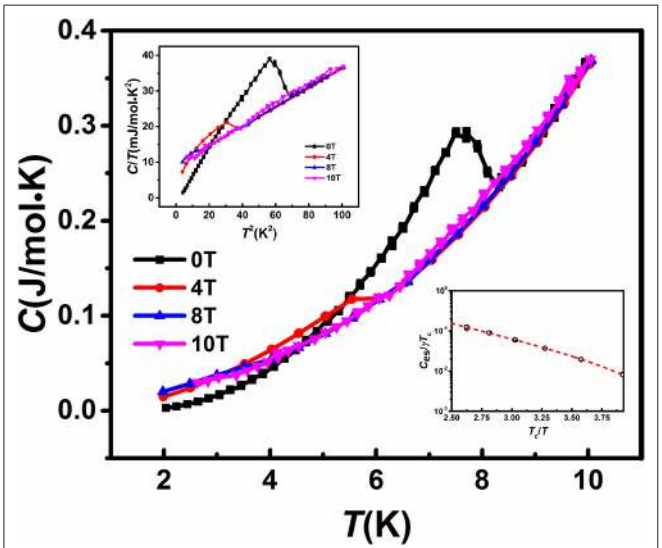

FIGURE 3 | $C(T)$of $Ti_{15}Zr_{15}Nb_{35}Ta_{35}$for H=0, 4, 8 and 10 T. The upper inset shows C/T vs T^2 under magnetic field. And the lower right inset is $C_{es}/\gamma T_C$ plotted on a logarithmic scale as a function of T_C/T.

state of a type-II superconductor (Awana et al., 2010). Based on the method reported in Ref. (Abdel-Hafiez et al., 2013), the lower critical field (H_{c1}) was obtained by measuring the virgin $M\,(H)$ curve at various temperatures, where the regression coefficient function $R\,(H)$ of a linear fit to the data between 0 and H departs from 1. Then the plot of $H_{c1}\,(T)$ is shown in the lower right inset of **Figure 4**. By linearly extrapolating $H_{c1}\,(T)$ to zero temperature, we obtain $H_{c1}\,(0) = 55$ mT. It should be noted that this is a very rough approximation in the absence of data at lower T.

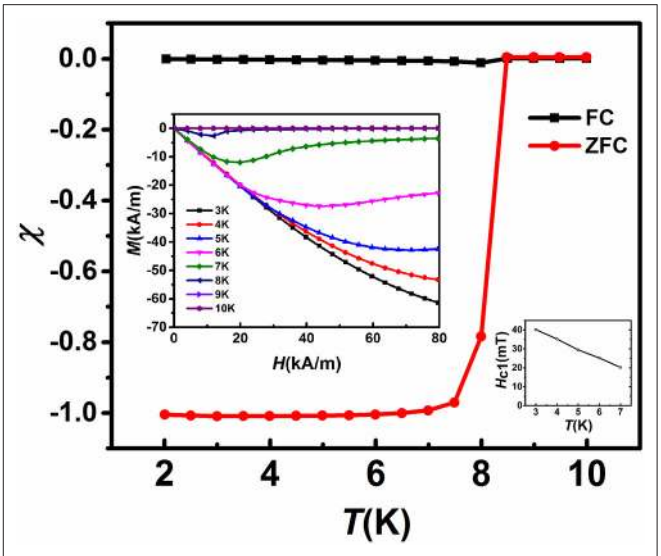

FIGURE 4 | Temperature dependence of magnetic susceptibility $\chi\,(T)$ measured under zero-field-cooled (ZFC) and field-cooled (FC) conditions at 3 mT for $Ti_{15}Zr_{15}Nb_{35}Ta_{35}$ samples. The left inset shows isothermal magnetization $M\,(H)$curves for $Ti_{15}Zr_{15}Nb_{35}Ta_{35}$ HEA at 3-10 K in the field range up to 80 kA/m. The lower right inset is the temperature dependence of the lower critical field$H_{c1}(T)$.

The upper critical field H_{c2} corresponding to the temperatures where the resistivity drops to 90% of the normal state resistivity $\rho(T, H)$ (see inset of **Figure 2**) at the onset critical temperature T_c^{onset} determined from the intersection of the two extrapolated lines of $\rho\,(T)$ in the applied magnetic fields (Jha et al., 2014). The upper critical field H_{c2} determined from resistivity (black circles) and from specific heat measurements (red squares) are shown in **Figure 5**. For a single-band superconductor in the dirty limit (Werthamer and Helfand, 1966; Wang et al., 2015), the orbital limit is given by $H_{c2}^{orb}\,(0) = -0.69\,dH_{c2}/dT\big|_{T=T_C} T_C$. Alternatively, the Pauli-limiting field for a weakly coupled BCS superconductor in the absence of spin-orbit scattering can be estimated as (Clogston, 1962) $H_P\,(0) = 1.86T_c$. The Maki parameter α is defined as $\alpha=\sqrt{2}H_{c2}^{orb}\,(0)\,/H_P\,(0)$. Assuming $T_C = 8.5$ K, and we have $dH_{c2}/dT\big|_{T=T_C} = -2$ T/K from **Figure 5**. Then α is calculated to be 1.05. We used the full Werthamer-Helfand-Hohenberg (WHH) formula that incorporates the spin-paramagnetic effect via the Maki parameter α and the spin-orbit scattering constant λ_{so} to describe the experimental H_{c2} data (Werthamer and Helfand, 1966):

$$\ln\frac{1}{t} = \sum_{\nu=-\infty}^{\infty}\left\{\frac{1}{|2\nu+1|} - \left[|2\nu+1| + \frac{\bar{h}}{t} + \frac{\left(\alpha\bar{h}/t\right)^2}{|2\nu+1| + \left(\bar{h}+\lambda_{so}\right)/t}\right]^{-1}\right\} \quad (1)$$

where $t = T/T_c$ and $\bar{h} = (4/\pi^2)\left[H_{c2}(T)/\left|dH_{c2}/dT\right|_{T_c}\right]$. As shown in **Figure 5**, the best fit can reproduce the experimental

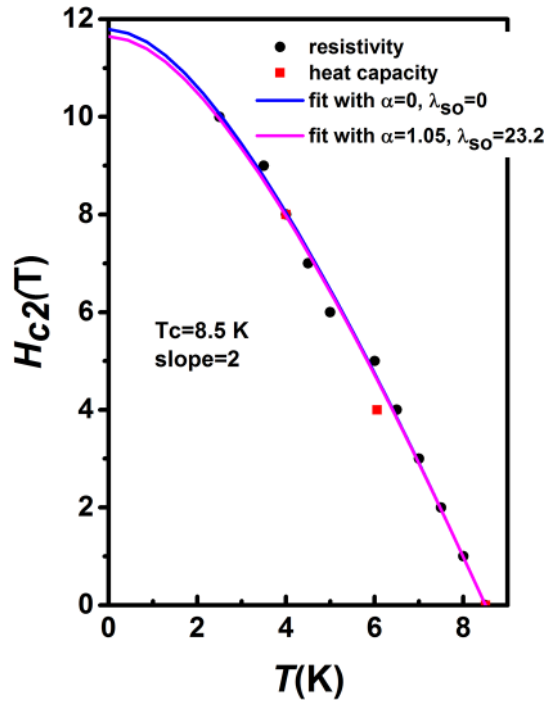

FIGURE 5 | The upper critical field H_{c2} from resistivity (black circles) and from specific heat measurements (red squares) as a function of temperature for the $Ti_{15}Zr_{15}Nb_{35}Ta_{35}$ HEA. The blue and pink lines are the WHH predictions with the parameter $\alpha = 0$, $\lambda_{so} = 0$, and $\alpha = 1.05$, $\lambda_{so} = 23.2$, respectively.

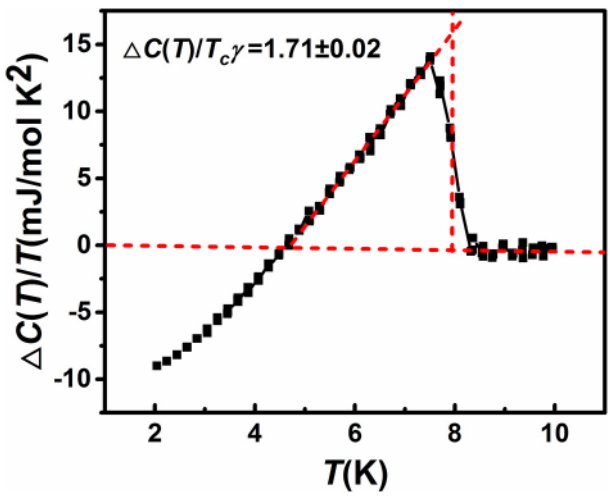

FIGURE 6 | $\Delta C(T)/T$ vs. T at $H = 0$ for the$Ti_{15}Zr_{15}Nb_{35}Ta_{35}$ HEA.

H_{c2} very well. By fixing $\alpha = 1.05$ to fit the H_{c2} data, we have $\lambda_{so} = 23.2$, $H_{c2}(0) = 11.6$ T. With these results for $H_{c1}(0)$ and $H_{c2}(0)$, we can calculate several SC parameters for our HEA. From $H_{c2} = \Phi_0/2\pi\xi_{GL}^2$, where Φ_0 is the quantum flux ($= h/2e = 2.07 \times 10^{-15}$ Wb), we find a Ginzburg-Landau coherence length $\xi_{GL}(0) = 53.3$ Å $= 5.33 \times 10^{-9}$ m. Assuming $\kappa = \lambda_{GL}/\xi_{GL}$ is temperature independent, then $\lambda_{GL}(0) = \kappa\xi_{GL}(0)$. Knowing$\xi_{GL}(0)$, $H_{c1}(0)$, and $H_{c1}(0) = \left(\Phi_0/4\pi(\kappa * \xi_{GL}(0))^2\right)\ln\kappa$, and hence the Ginzburg-Landau parameter, $\kappa = 17.3$.

With respect to the superconductivity in $Ti_{15}Zr_{15}Nb_{35}Ta_{35}$ HEA, the most interesting part is the detailed analysis of the anomaly in the specific heat $C(T)$. The low-temperature specific heat in the normal state is expressed as $C(T) = \gamma T + C_{lattic}(T)$, where the electronic specific heat coefficient γ measures the degree of electronic contribution and $C_{lattic}(T) = \beta T^3 + \sigma T^5$ represents the phonon contribution in which β is the lattice specific heat coefficient. Then the plot of C/T vs. T^2 is shown in the upper inset of **Figure 3**. The analysis of the normal-state specific heat (in 8 or 10 T field) with the expression $C/T = \gamma + \beta T^2$ yields the intercept $\gamma = 9.3 \pm 0.1$ mJ/mol K^2, the slope $\beta = 0.28 \pm 0.01$ mJ/mol K^4 and the Debye temperature $\theta_D = (12\pi^4 R/5\beta)^{1/3} = 191 \pm 3$ K. Clearly, for the current HEA, the electronic specific heat coefficient γ increases by about 12% as compared with that of the reported $Ta_{34}Nb_{33}Hf_8Zr_{14}Ti_{11}$ HEA.

To elucidate the nature of the SC state of the$Ti_{15}Zr_{15}Nb_{35}Ta_{35}$ HEA, e.g., Bardeen-Cooper-Schrieffer (BCS) type (Bardeen et al., 1957) or unconventional, it is of interest to calculate the discontinuous jump of specific heat at the SC transition temperature, i.e., $\Delta C(T) = C(T) - C_{lattice}(T) - \gamma T$. The resultant $\Delta C(T)/T$ at $H = 0$ is shown in **Figure 6**. Utilizing the balance of entropy around the transition, $\Delta C/\gamma T_c$ (the specific-heat jump) is 1.71 ± 0.02 for the current HEA which deviates appreciably from that for a weak electron-phonon coupling BCS superconductor ($\Delta C/\gamma T_c = 1.43$).

Based on the BCS theory (Tinkham, 2004), the energy required to break up a Cooper pair is about $2\Delta_0$, and the number of Cooper pairs broken up is proportional to $\exp\left(-2\Delta(0)/k_BT\right)$, which leads an exponential temperature dependence of the specific heat at sufficiently low temperature. The electronic specific heat $C_{es}(T)$ [$C_{es}(T) = C(T,H) - C_{lattice}(T)$] in the BCS theory is expressed by $C_{es}/\gamma T_c = A\exp(-BT_c/T)$ (Tari, 2003), where A and B are two constants whose values relate to the temperature interval used. Evidently in the lower inset of **Figure 3**, $C_{es}(T)$of the $Ti_{15}Zr_{15}Nb_{35}Ta_{35}$ HEA reflects clearly an exponential behavior. The fit $C_{es}(T)$ of the current HEA at $2.5 < T_C/T < 6$ yields $C_{es}/\gamma T_c = 10.1 \times \exp(-1.66T_c/T)$. Evidently, it does have the characteristics of exponential behavior predicted by the BCS theory, but the factors are far from the weak electron-phonon coupling (Takeya et al., 2005).This phenomenon is different from the reported $Ta_{34}Nb_{33}Hf_8Zr_{14}Ti_{11}$ HEA (Koželj et al., 2014).

It is found that the measured SC properties in $Ti_{15}Zr_{15}Nb_{35}Ta_{35}$ HEA agree extremely well with the following strong electron-phonon coupling corrections (valid for $T_c/\omega_{\log} << 1$, where $\omega_{\log}$ is a characteristic phonon temperature; McMillan, 1968; Ishikawa and Toth, 1971; Allen and Dynes, 1975; Carbotte, 1990):

$$[\Delta C/\gamma T_c]_{T_c} = 1.43\left[1 + 53\left(T_c/\omega_{\log}\right)^2 \ln(\omega_{\log}/3T_c)\right] \quad (2)$$

$$2\Delta_0/k_BT_c = 3.53\left[1 + 12.5\left(T_c/\omega_{\log}\right)^2 \ln\left(\omega_{\log}/2T_c\right)\right] \quad (3)$$

TABLE 2 | SC parameters of $Ti_{15}Zr_{15}Nb_{35}Ta_{35}$ HEA and the reported $Ta_{34}Nb_{33}Hf_8Zr_{14}Ti_{11}$ HEA (Koželj et al., 2014).

Composition	Experiment				Calculation				
	T_c(K)	γ (mJ/mol K^2)	θ_D(K)	$\Delta C/\gamma T_c$	ω_{log}(K)	T_c/ω_{log}	$2\Delta_0$(meV)	λ	$N(E_F)$(1/eV/fu)
$Ti_{15}Zr_{15}Nb_{35}Ta_{35}$	8.0	9.3 ± 0.1	191 ± 3	1.71 ± 0.02	189 ± 10	0.042 ± 0.003	2.57 ± 0.01	0.84 ± 0.02	1.07 ±0.01
$Ta_{34}Nb_{33}Hf_8Zr_{14}Ti_{11}$	7.3	8.3 ± 0.1	243 ± 5	1.63 ± 0.06			2.2	0.66 ± 0.01	1.06 ±0.02

The corresponding strong-coupling corrections [Equations (2–4)] are used for the calculation on $Ti_{15}Zr_{15}Nb_{35}Ta_{35}$ HEA.

$$T_c = \frac{\omega_{\log}}{1.2} \exp\left(-\frac{1.04\,(1+\lambda)}{\lambda - \mu^*\,(1+0.62\lambda)}\right) \quad (4)$$

where $k_B$is the Boltzmann constant, λ the electronic-phonon coupling parameter, and μ^* the Coulomb pseudopotential taken to be 0.13 here, which is an average value used commonly for intermetallic superconductors (Klimczuk et al., 2012; von Rohr et al., 2016). The values of $\omega_{\log}$,$2\Delta_0$ and λ were determined by Equations (2–4) based on the experimentally measured$\Delta C/\gamma T_c$, as compiled in **Table 2**. It is apparent that the calculated results are reasonably satisfied with the condition $T_c/\omega_{\log} << 1$. The value of $2\Delta_0/k_BT_c$ is 3.52 for the weak-coupling BCS conventional superconductors. In our HEA, $2\Delta_0/k_BT_c$is calculate to be 3.72 ± 0.02 using the energy gap $2\Delta_0$ of 2.57 ± 0.01 meV, larger than the reported Ta $_{34}Nb_{33}Hf_8Zr_{14}Ti_{11}$ HEA of 3.50 indicating the stronger electron-phonon coupling (Takeya et al., 2005). Therefore, these values suggest that the $Ti_{15}Zr_{15}Nb_{35}Ta_{35}$ HEA is an intermediate-coupled superconductor, when compared with the reported weak-coupled Ta $_{34}Nb_{33}Hf_8Zr_{14}Ti_{11}$ HEA.

The electronic-phonon coupling parameter λ in the reported weak-coupling $Ta_{34}Nb_{33}Hf_8Zr_{14}Ti_{11}$ HEA is calculated to be 0.66 ± 0.01 using the equation $T_c = (\theta_D/1.45)\exp[-(1+\lambda)/(\lambda-\mu^*)]$ (Takeya et al., 2005). Clearly this value of λ is lower than that of the current HEA (0.84 ± 0.02). The electron density of state at the Fermi level $N(E_F)$ is estimated to be 1.07 ± 0.01 and 1.06 ± 0.02 by $\gamma = \frac{2}{3}\pi^2 k_B^2 (1+\lambda) N(E_F)$for the$Ti_{15}Zr_{15}Nb_{35}Ta_{35}$ HEA and the reported $Ta_{34}Nb_{33}Hf_8Zr_{14}Ti_{11}$HEA, respectively. Therefore, the improvement of SC temperature T_c is related to the increase of the electron density of state at the Fermi level$N(E_F)$. In addition, the electron-phonon coupling is enhanced, which also might contribute to the increase of T_c. It was also found in the current HEA that the SC properties, e.g., T_c and γ ,do not obey the Vegard's rule of mixture (Vegard, 1921), $p_{mix} = \sum_{i=1}^{n} c_i p_i$, where c_i and p_i are the atomic percentage and the SC property of each constituent element (**Table 1**), respectively. This observation suggests that electronic properties are not a "cocktail" of properties of the constituent elements. Theoretical description of the electronic properties of HEAs is thus a highly complex problem.

CONCLUSIONS

The $Ti_{15}Zr_{15}Nb_{35}Ta_{35}$ HEA with a single BCC lattice was synthesized and found to be a type-II superconductor. The analysis of all the specific heat data shows that this new $Ti_{15}Zr_{15}Nb_{35}Ta_{35}$HEA is a BCS-type phonon-mediated superconductor in the intermediate electron-phonon coupling regime, which is different from the previous report. Despite the complex electronic properties, our results also indicate that the characteristics of superconductivity of HEAs can be tailored by varying their chemical composition. Further experiments on its transport properties under high pressure would be very interesting to check the robustness of superconductivity.

AUTHOR CONTRIBUTIONS

YY performed the experiments. YW, HL, ZW, XL, ZY, HW, XL, and ZL supervised the project. YY, HL, and ZW analyzed the data. YY, YW, and ZL wrote the paper. All authors commented on the manuscript.

ACKNOWLEDGMENTS

This research was supported by National Natural Science Foundation of China (Nos. 11790293, 51871016, 51671018, 51671021, 51531001 11822411, 11674372, 11704385 and 11874359), 111 Project (B07003), International S&T Cooperation Program of China (2015DFG52600), Program for Changjiang Scholars and Innovative Research Team in University of China (IRT_14R05), and the Projects of SKLAMM-USTB (2016Z-04, 2016-09, 2016Z-16). YW acknowledges the financial support from the Top-Notch Young Talents Program and Fundamental Research Fund for the Central Universities. HL acknowledges the financial support from the Chinese Academy of Sciences (SPRP-B: XDB25000000 and the Youth Innovation Promotion Association).

REFERENCES

Abdel-Hafiez, M., Ge, J., Vasiliev, A., Chareev, D., Van de Vondel, J., Moshchalkov, V., et al. (2013).Temperature dependence of lower critical field $H_{c1}(T)$ shows nodeless superconductivity in FeSe. *Phys. Rev. B* 88:174512. doi: 10.1103/PhysRevB.88.174512

Allen, P. B., and Dynes, R. (1975). Transition temperature of strong-coupled superconductors reanalyzed. *Phys. Rev. B* 12:905. doi: 10.1103/PhysRevB.12.905

Ashcroft, N., and Mermin, N. (1976). Solid State Physics (Saunders, Philadelphia). *Phil. Mag.* 3:445.

Awana, V., Pal, A., Vajpayee, A., Meena, R., Kishan, H., Husain, M., et al. (2010). Superconductivity in $SmFe_{1-x}Co_xAsO$ (x=0.0-0.30). *J. Appl. Phys.* 107:09E146. doi: 10.1063/1.3366601

Bardeen, J., Cooper, L. N., and Schrieffer, J. R. (1957). Theory of superconductivity. *Phys. Rev.* 108:1175. doi: 10.1103/PhysRev.108.1175

Brown, W. F. Jr. (1960). Single-domain particles: new uses of old theorems. *Am. J. Phys.* 28, 542–551. doi: 10.1119/1.1935878

Carbotte, J. (1990). Properties of boson-exchange superconductors. *Rev. Mod. Phys.* 62:1027. doi: 10.1103/RevModPhys.62.1027

Chuang, M. H., Tsai, M. H., Wang, W. R., Lin, S. J., and Yeh, J. W. (2011). Microstructure and wear behavior of $Al_xCo_{1.5}CrFeNi_{1.5}Ti_y$ high-entropy alloys. *Acta Mater.* 59, 6308–6317. doi: 10.1016/j.actamat.2011.06.041

Clogston, A. M. (1962). Upper limit for the critical field in hard superconductors. *Phys. Rev. Lett.* 9:266. doi: 10.1103/PhysRevLett.9.266

Conrad, M., Harbrecht, B., Weber, T., Jung, D. Y., and Steurer, W. (2009). Large, larger, largest–a family of cluster-based tantalum copper aluminides with giant unit cells. *II. The cluster structure. Acta Crystallogr. Sect. B Struct. Sci.* 65, 318–325. doi: 10.1107/S0108768109014013

Crabtree, G. (1977). Demagnetizing fields in the de Haas-van Alphen effect. *Phys. Rev. B* 16:1117. doi: 10.1103/PhysRevB.16.1117

Guo, J., Wang, H., von Rohr, F., Wang, Z., Cai, S., Zhou, Y., et al. (2017). Robust zero resistance in a superconducting high-entropy alloy at pressures up to 190 GPa. *PNAS* 114:13144. doi: 10.1073/pnas.1716981114

Hsu, C. Y., Juan, C. C., Wang, W. R., Sheu, T. S., Yeh, J. W., and Chen, S. K. (2011). On the superior hot hardness and softening resistance of $AlCoCr_xFeMo_{0.5}Ni$ high-entropy alloys. *Mater. Sci. Eng. A* 528, 3581–3588. doi: 10.1016/j.msea.2011.01.072

Ishikawa, M., and Toth, L. E. (1971). Electronic specific heats and superconductivity in the group-*V* transition metals. *Phys.Rev. B* 3:1856. doi: 10.1103/PhysRevB.3.1856

Jha, R., Kishan, H., and Awana, V. (2014). Superconducting and magneto-transport properties of BiS2 based superconductor $PrO_{1-x}F_xBiS_2$ (x= 0 to 0.9). *J. Appl. Phys.* 115:013902. doi: 10.1063/1.4859535

Klimczuk, T., Wang, C., Gofryk, K., Ronning, F., Winterlik, J., Fecher, G., et al. (2012). Superconductivity in the Heusler family of intermetallics. *Phys. Rev. B* 85:174505. doi: 10.1103/PhysRevB.85.174505

Koželj, P., Vrtnik, S., Jelen, A., Jazbec, S., Jaglicić, Z., Maiti, S., et al. (2014). Discovery of a superconducting high-entropy alloy. *Phys. Rev. Lett.* 113:107001. doi: 10.1103/PhysRevLett.113.107001

Li, D. Y., Li, C. X., Feng, T., Zhang, Y. D., Sha, G., Lewandowski, J. J., et al. (2017). High-entropy $Al_{0.3}CoCrFeNi$ alloy fibers with high tensile strength and ductility at ambient and cryogenic temperatures. *Acta Mater.* 123, 285–294. doi: 10.1016/j.actamat.2016.10.038

Lu, Z. P., Wang, H., Chen, M. W., Baker, I., Yeh, J. W., Liu, C. T., et al. (2015). An assessment on the future development of high-entropy alloys: summary from a recent workshop. *Intermetallics* 66, 67–76. doi: 10.1016/j.intermet.2015.06.021

McMillan, W. (1968). Transition temperature of strong-coupled superconductors. *Phys. Rev.* 167:331.doi: 10.1103/PhysRev.167.331

Senkov, O., Scott, J., Senkova, S., Miracle, D., and Woodward, C. (2011). Microstructure and room temperature properties of a high-entropy TaNbHfZrTi alloy. *J.Alloys Compd.* 509, 6043–6048.doi: 10.1016/j.jallcom.2011.02.171

Senkov, O., Wilks, G., Miracle, D., Chuang, C., and Liaw, P. (2010). Refractory high-entropy alloys. *Intermetallics* 18, 1758–1765. doi: 10.1016/j.intermet.2010.05.014

Takeya, H., Hirata, K., Yamaura, K., Togano, K., El Massalami, M., Rapp, R., et al. (2005). Low-temperature specific-heat and neutron-diffraction studies on Li_2Pd_3B and Li_2Pt_3B superconductors. *Phys. Rev. B* 72:104506.doi: 10.1103/PhysRevB.72.104506

Tari, A. (2003). *The Specific Heat of Matter at Low Temperatures*. London: Imperial College Press.

Tinkham, M. (2004). *Introduction to Superconductivity*. North Chelmsford, MA: Courier Corporation.

Todai, M., Nagase, T., Hori, T., Matsugaki, A., Sekita, A., and Nakano, T. (2017). Novel TiNbTaZrMo high-entropy alloys for metallic biomaterials. *Scr. Mater.* 129, 65–68. doi: 10.1016/j.scriptamat.2016.10.028

Urban, K., and Feuerbacher, M. (2004). Structurally complex alloy phases. *J. Non-Cryst. Solids* 334, 143–150. doi: 10.1016/j.jnoncrysol.2003.11.029

Vegard, L. (1921). Die konstitution der mischkristalle und die raumfüllung der atome. *Zeitschrift Physik* 5, 17–26.

von Rohr, F., Winiarski, M. J., Tao, J., Klimczuk, T., and Cava, R. J. (2016). Effect of electron count and chemical complexity in the Ta-Nb-Hf-Zr-Ti high-entropy alloy superconductor. *PNAS* 113, E7144–E7150. doi: 10.1073/pnas.1615926113

Wang, Z., Xie, T., Kampert, E., Förster, T., Lu, X., Zhang, R., et al. (2015). Electron doping dependence of the anisotropic superconductivity in $BaFe_{2-x}Ni_xAs_2$. *Phys. Rev. B* 92:174509. doi: 10.1103/PhysRevB.92.174509

Wen, L., Kou, H., Li, J., Chang, H., Xue, X., and Zhou, L. (2009). Effect of aging temperature on microstructure and properties of AlCoCrCuFeNi high-entropy alloy. *Intermetallics* 17, 266–269. doi: 10.1016/j.intermet.2008.08.012

Werthamer, N. R., and Helfand,E. andHohenberg, P. C. (1966). Temperature and purity dependence of the superconducting critical field, *Hc*2. III. electron spin and spin-orbit effects. *Phys. Rev.* 147:295.

Yeh, J. W. (2006). Recent progress in high entropy alloys. *Ann. Chim. Sci. Mat* 31, 633–648. doi: 10.3166/acsm.31.633-648

Yeh, J. W., Chen, S. K., Lin, S. J., Gan, J. Y., Chin, T. S., Shun, T. T., et al. (2004). Nanostructured high-entropy alloys with multiple principal elements: novel alloy design concepts and outcomes. *Adv. Eng. Mater.* 6, 299–303. doi: 10.1002/adem.200300567

Zhou, Y., Zhang, Y., Wang, Y., and Chen, G. (2007). Solid solution alloys of $AlCoCrFeNiTi_x$ with excellent room-temperature mechanical properties. *Appl. Phys. Lett.* 90:1904. doi: 10.1063/1.2734517

Conflict of Interest Statement: The authors declare that the research was conducted in the absence of any commercial or financial relationships that could be construed as a potential conflict of interest.